Radio Science

RESEARCH ARTICLE
10.1029/2020RS007155

Key Points:
- The high data accuracy and ambitious objectives of RISE and LaRa experiments led us to provide a Mars troposphere error correction model
- The model provides zenith and slant delays, radial velocity, and Doppler shifts induced by Mars neutral atmosphere
- The model is used to compute corrections to apply to the X-band data provided by the Martian rover and lander missions, including InSight

Correspondence to:
S. Le Maistre,
sebastien.lemaistre@oma.be

Citation:
Le Maistre, S. (2020). Martian lander radio science data calibration for Mars troposphere. *Radio Science*, *55*, e2020RS007155. https://doi.org/10.1029/2020RS007155

Received 3 JUL 2020
Accepted 14 NOV 2020
Accepted article online 4 DEC 2020

Martian Lander Radio Science Data Calibration for Mars Troposphere

S. Le Maistre[1]

[1]Royal Observatory of Belgium, Uccle, Belgium

Abstract The tropospheric propagation effect is one of several sources of error in radio science measurements. Systematically calibrated for the Earth troposphere disturbances, the ranging and Doppler data provided by the Martian landers have not been corrected so far for Mars troposphere effects. These effects were considered negligible because the Mars atmosphere is a hundred times less dense than that of the Earth. The constantly improving lander data accuracy and the challenging science objectives of the InSight-Rotation and Interior Structure Experiment (RISE) and ExoMars-2022-LaRa radio science experiments motivated this work. We propose here a simple model to compute the Mars troposphere errors affecting a radio wave transponded from the surface of Mars. The troposphere zenithal delay is first derived from the surface pressure at the lander location. We use a mapping function to infer the slant delay (range errors) induced by the troposphere of Mars. Being proportional to range rates, the contribution of Mars troposphere to the Doppler measurements is derived from the slant delays. Using our model, an elevation threshold of 15° above the lander is identified, below which the Doppler data should be calibrated for Mars troposphere. When applied to the X-band Doppler data from Mars surface missions, the model predicts significant Mars troposphere contribution for less than 1% of RISE data, 2% of Opportunity data, and 2.5% of Pathfinder data. Among these tracking passes, some are strongly affected by the troposphere of Mars, with Doppler errors reaching sometimes more than 3 times the nominal noise level (>10 mHz at 60 s integration time).

1. Introduction

Since a few decades radio science exhibits a rich and varied evolution leading to knowledge of interior, atmosphere, and surface parameters. Radio science data rely on radio links between two spacecraft or between a spacecraft and an Earth ground station. For deep space missions like the ones involving a lander on Mars, National Aeronautics and Space Administration (NASA) uses its Deep-Space-Network (DSN) antennas and European Space Agency (ESA) uses its ESTRACK network of stations to track the probe directly from Earth. The radio-tracking data so obtained mainly consist of Doppler and range measurements. These measurements are affected by noises of various sources (see Asmar et al., 2005, for more details) such as the instrumental noises (related to ground and spacecraft electronics, mechanical parts, and radio link finite signal-to-noise ratio), systematic errors (e.g., antenna focusing errors), and propagation noises. The propagation noises are random frequency/phase fluctuations caused by refractive index fluctuations along the line of sight (LOS). The refractive index characterizes the media through which the radio wave passes, such as the solar wind or the Earth troposphere and ionosphere. For Mars surface observations (or for orbiter radio occultation measurements), the planet's troposphere and ionosphere also induce phase/frequency fluctuations. Those Mars atmospheric disturbances have been ignored so far in the analysis of Martian landers radio science data (e.g., Folkner et al., 1997; Kuchynka et al., 2014; Le Maistre, 2013). However, radio science instrument performances are constantly improving (e.g., S-band Viking data were about 3 times less accurate than the X-band Opportunity data) and the forthcoming data are expected to be more and more accurate. The Rotation and Interior Structure Experiment (RISE) (Folkner et al., 2018), payload of the NASA InSight mission operating from the surface of Mars since 26 November 2018, provides Doppler data more accurate (Kahan et al., 2021) than considered in the simulation studies (Péters et al., 2020) and that should be comparable to those of the future Lander Radio science (LaRa) experiment. LaRa is a scientific payload of the Russian surface platform to be delivered on the surface of Mars in June–July 2023 by the ESA-Roscosmos ExoMars 2022 mission (Dehant et al., 2020). The measurements of RISE and LaRa provide the Doppler shift with a couple of mHz of precision when integrated over 60 s. Moreover, RISE nominal range of LOS

10.1029/2020RS007155

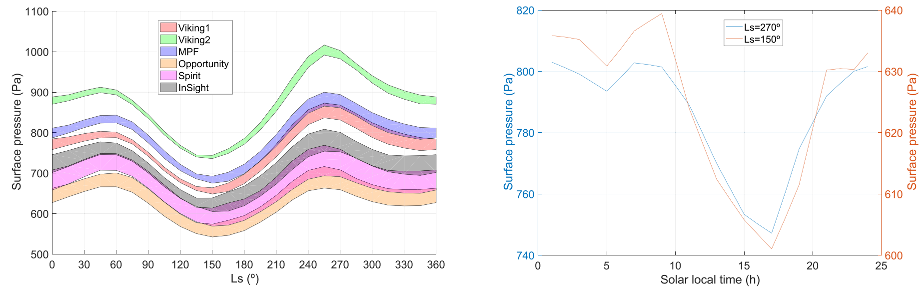

Figure 1. MCD-computed surface pressure (P_S) as a function of Mars solar longitude (Ls) for different sites corresponding to the lander locations (left) and the solar local time at Insight location (right). The thickness of the colored areas in the left panel is the range of pressure within the day between 9 a.m. and 3 p.m., typical tracking time of InSight's RISE.

elevation during tracking is 10–30°. This is quite low, making the wave traveling through a thicker layer of Mars atmosphere and consequently more affected by the Mars atmospheric noise than if it was coming from the lander's zenith. LaRa is designed to nominally operate at 35–45° elevation (Le Maistre et al., 2020; Péters et al., 2020), which should avoid significant Mars atmospheric noise. Nevertheless, for programmatic reasons or in case of an unfortunate large tilt of the ExoMars' surface platform, it is likely that LaRa observations will also be carried out sometimes at low elevations, as it has been the case for the previous lander and rover missions (Le Maistre, 2013). All this, along with the challenging objectives of those lander missions, namely, the determination of tiny (approximately cm level) variations in the planet's orientation, motivated us to take a closer look at Mars atmospheric disturbances on the Martian lander radio-tracking data. Mars ionosphere has recently been studied by Bergeot et al. (2019), who provided an empirical model based on Mars Express's MARSIS radar data, from which they predicted a contribution (i.e., a Mars ionosphere noise) to the X-band Doppler measurements to be lower than 0.05 mHz and a contribution to the X-band range measurements to be below 2 cm. Not studied in details so far, the Mars tropospheric noise is quantified in the present work.

We first succinctly present the characteristics of the Mars troposphere (section 2). We then recall the basic equations of the radio wave propagation delay (section 3), and we describe a simple model to compute the Mars troposphere zenithal delay (section 4). After a brief discussion on the mapping functions allowing to compute the slant delay (section 5), we provide a method to correct lander's Doppler and range data from Mars tropospheric noise (section 6). These model and method are finally applied to X-band Doppler data of the Martian landers and rover (section 7). Section 8 gathers the conclusions of the paper.

2. Mars Troposphere

Planetary atmosphere layers are concentric layers characterized by features like temperature or ionization. The characteristics of propagation of a wave through the atmosphere are a criterium that can also be used to subdivide the atmosphere of a planet. In such a case, the upper part is the ionosphere and the lower part is an electrically neutral and non-dispersive medium, perturbing the propagation of an electromagnetic wave independently from its frequency. As it is commonly the case in radio science, troposphere refers in this study to the neutral layer of the atmosphere.

Mars atmosphere is much thinner than that of Earth, with a mean temperature of same order of magnitude, and a pressure at the surface averaging 1/100 that at the surface of the Earth. The barometric pressure significantly varies on a semiannual basis, with an amplitude of about 15% of the 6–9 mbar of mean pressure, and in a minor extent on a diurnal basis (e.g., Haberle et al., 2017). This behavior is shown in Figure 1, obtained using the Mars Climate Database (MCD) (Forget et al., 1999; Millour et al., 2018).

Mars atmospheric composition is very different from that of the Earth, with 95.32% of CO_2, 2.7% of N_2, 1.6% of Ar, and less than 0.4% of other constituents (Owen et al., 1977). Unlike the Earth, Mars atmosphere is really dry and the water vapor mixing ratio hardly reaches a peak value of 3E−03 at the North Pole around Mars longitude Ls = 90°. This corresponds to a maximum in the partial pressure of water vapor P_{wt} of ∼2–3 Pa, that is, 0.3% of the total pressure of Mars atmosphere (see Montmessin et al., 2017, and reference

10.1029/2020RS007155

therein). The mean value of P_{wt} is about 1 order of magnitude lower than that, as can be concluded given that H_20 is 100–200 ppm of Mars atmosphere volume (see, for instance, Figure 5 of Rodin et al., 1997).

Because Mars atmosphere is so dry, its gas constituents nearly behave as perfect gas, which makes the propagation delay model simpler and more accurate. The fact that Mars atmosphere is so tenuous led to expect low level of propagation perturbations in Mars troposphere. Nevertheless, as shown below, this level is sometimes higher than the current measurement accuracy level and needs to be examined.

3. Radio Wave Propagation Delay

The propagation delay induced by the electrically neutral atmosphere, recognized as the main source of error for radiometric space geodetic techniques on Earth, have been deeply studied over the past decades. This led to a clear understanding and accurate modelings of the propagation delay experienced by a radio wave in the Earth troposphere (e.g., Mendes, 1999). We here use similar models as those used for the Earth but simple enough to be applied to the less monitored Mars troposphere.

The distance traveled by a radio wave passing through the troposphere layer is (e.g., Kleijer, 2004)

$$L_\tau = \int_{path} cdt = \int_{path} n(s)ds, \tag{1}$$

where c is the speed of light in vacuum, $n(s) = c/v(s)$ is the refraction index of Mars troposphere, $v(s)$ is the signal propagation speed in the troposphere, and ds is an increment of distance along the electromagnetic path. We denote the geometric distance by

$$L_g = \int_{vac} dl, \tag{2}$$

where dl is an increment of distance along the geometrical path that would be used by the ray if propagating in vacuum. The excess path length due to Mars troposphere, d_τ, inappropriately named "delay" in the rest of the paper, can be obtained by subtracting these two distances:

$$d_\tau = L_\tau - L_g = \int_{path} (n(s) - 1)\, ds + \left(\int_{path} ds - \int_{vac} dl \right). \tag{3}$$

The first term in the right-hand side is the excess path length caused by the propagation delay, whereas the second term (in parenthesis) is the excess path length caused by ray bending. The second term is several orders of magnitude smaller than the first one with an exponentially decreasing-with-elevation delay as small as ~1 mm at 15° elevation in the Earth troposphere (Mendes, 1999). Therefore, this term is neglected when computing the radio signal extra distance due to propagation speed reduction (i.e., n, N increase) in the planet troposphere, which reads

$$d_\tau = 10^{-6} \int_{path} Nds. \tag{4}$$

All along the paper we use subscript or superscript τ to specify that the considered quantity (here the excess path length, d) is induced by the troposphere of Mars.

As is customary (e.g., Smith & Weintraub, 1953), because n is close to one, we made in the above equation the change of variable $N = 10^6(n - 1)$, where N is the dimensionless refractivity. N is used to describe the spatial and temporal variation of the planet's air refractive index.

The Earth troposphere contains both dry air and water vapor in a significant amount, such that the Earth troposphere refractivity is usually split into a dry and a wet part: $N = N_{dr} + N_{wt}$. Assuming dry air and water vapor to be ideal gases with unit compressibility factors, the refractivities can be expressed as a function of temperature T (in kelvins) and partial pressures P (in millibars) (Smith & Weintraub, 1953):

$$N_{dr} = k_1 \frac{P_{dr}}{T}, \tag{5}$$

$$N_{wt} = k_2 \frac{P_{wt}}{T^2}. \tag{6}$$

Table 1
Mars Parameters and Constants

Parameter	Symbol	Value	Unit	Reference
Universal gas constant	R_g	8.31446261815324	J/K/mol	—
Gravitational parameter	GM	42,828.374	km^3/s^2	Konopliv et al. (2011)
Equatorial radius	R_e	3,396.19	km	Archinal et al. (2018)
Mean surface gravity	g_0	3.71	m/s^2	GM/R_e^2
Mean surface temperature	T_0	210	K	Ho et al. (2002)
Mean surface pressure	P_0	650	Pa	MCD (Millour et al., 2018)
Mean partial pressure of water vapor	P_w	0.3	Pa	MCD (Millour et al., 2018)
Refractivity constant	k_1	130.6	K/mbar	Ho et al. (2002)
Refractivity constant	k_2	3.73E−05	K^2/mbar	Ho et al. (2002)
Troposphere scale height	H	11.1	km	Ho et al. (2002)
Mean surface dry refractivity	N_{dr}	4	—	Equation 5
Mean surface wet refractivity	N_{wt}	10^{-10}	—	Equation 6
CO_2 molar mass	M_{CO_2}	44.01	g/mol	—
N_2 molar mass	M_{N_2}	28.02	g/mol	—
Ar molar mass	M_{Ar}	39.95	g/mol	—
Total molar mass	M	43.34	g/mol	Equation 8

Subscripts dr and wt stand for dry and wet components, respectively. k_1 and k_2 are empirical constants reported in Table 1 for Mars. They have been computed from refractivity at standard temperature and pressure of each constituent gas of the atmosphere and its fractional abundance by volume in the atmosphere. More details about the computation of these constants can be found in Withers (2010), for instance, as well as the values of k_1 for most of the solar system atmospheres.

As said before, the Martian neutral atmosphere is mostly free of water vapor, with $P_{wt} \simeq 0.3$ Pa in average. According to the numerical values (Table 1) of the quantities used to compute the refractivities (Equations 5 and 6), one can show that the wet refractivity is in average 10 orders of magnitude smaller than the dry refractivity. This leads us to ignore the wet component and reduce N to $N = N_{dr}$.

The dry refractivity at the lander location can be accurately computed based on reliable surface pressure and temperature data since the laws of temperature and pressure decreasing with altitude are well known (assuming perfect gas). Because such pressure and temperature data characterize the column of atmosphere above the lander location, the so-obtained refractivity is denoted N_{dr}^z (superscript z for zenithal). Substituting N_{dr}^z for N in Equation 4, the zenithal dry (or hydrostatic) delay (d_{dr}^z) experienced by a signal arriving from the lander's zenith can be computed.

4. Zenithal Delay Model

On combining the equation describing hydrostatic balance with the ideal gas law, one can show that, in an isothermal atmosphere, the pressure and density fall exponentially with altitude.

Gravity thus tends to produce a density stratification in the atmosphere and N, which is proportional to the neutral number density, also decreases exponentially with increasing altitude z (e.g., Andrews, 2010). Assuming an isothermal Mars troposphere (i.e., dry troposphere of constant temperature) in hydrostatic equilibrium, the vertical pressure profile can simply be modeled as

$$P(z) = P_s e^{-\frac{g_s M}{R_g T_s} z}, \tag{7}$$

where $P(z)$ is the pressure at height z above the surface, P_s is the local surface pressure (or pressure at adjacent level), T_s is the local surface temperature, g_s is the local surface gravity acceleration, R_g is the universal gas constant, and M is the molar mass of the dry atmosphere (see numerical values for Mars in Table 1).

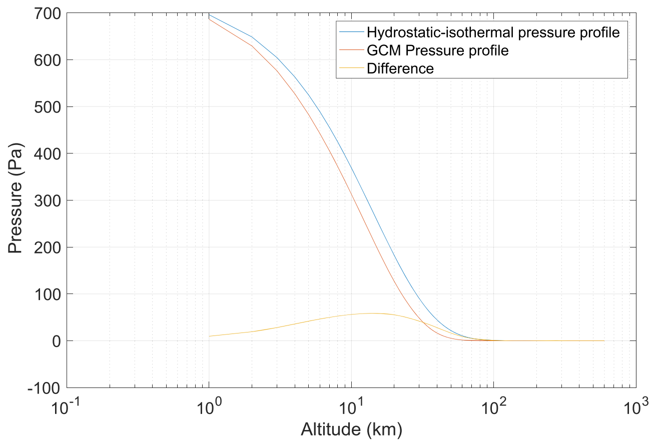

Figure 2. Mars atmosphere vertical pressure profiles computed at InSight location.

M is equal to the sum of the molar mass M_i of the ith constituents of Mars atmosphere times f_i, its number density (i.e., its fractional abundance by volume):

$$M = \sum_i f_i M_i \simeq 0.9532 M_{CO_2} + 0.027 M_{N_2} + 0.016 M_{Ar}. \quad (8)$$

The pressure model of Equation 7 is well representing the behavior of real non-isothermal Mars atmosphere as suggested by Figure 2 where the model is superimposed with pressure profile provided by the MCD (Millour et al., 2018), with a discrepancy maximized to ~50 Pa (0.5 mbar) at about 15 km altitude and totally negligible above 100 km altitude.

By replacing P_{dr} by $P(z)$ in Equation 5 and then injecting N^z_{dr} in place of N in Equation 4, the zenithal tropospheric (dry) delay (d^z_τ) can be computed. The integration of N^z_{dr} over the height z is straightforward when one assumes that $\forall z$, $T(z) = T_s$, and the result is

$$d^z_\tau = k_1 \frac{P_s R_g}{g_s M} \left[1 - e^{-\frac{g_s M}{R_g T_s} z} \right] = k_1 \frac{R_g}{g_s M} \left(P_s - P(z) \right). \quad (9)$$

According to Equations 7 and 9, the (pressure) scale height H, which corresponds to the height over which the pressure falls by a factor of e, is $H = R_g T_s / (g_s M)$. Considering the average values of Mars surface temperature (i.e., $T_s = T_0$) and surface gravity (i.e., $g_s = g_0 = GM/R_e^2$, with R_e the Mars equatorial radius, see Table 1), we get $H \simeq 11$ km. This means that the pressure, and subsequently the refractivity and the zenithal delay decrease by 95% of their surface value at $z = 6H \simeq 66$ km. For a receiver that would be at a very low altitude (i.e., around 5–30 km), d^z_τ would be influenced by the surface temperature via $P(z)$, while above 50 km the temperature effect would be very small, as shown in bottom panels of Figure 3. In practical, the radio signal is propagating from/to the surface to/from the outside of the Mars atmosphere (i.e., $z \gg H$), which makes $P(z) = 0$ at altitude z of the receiver (being the Earth in case of direct-to-Earth data, or an orbiter at altitude $z > 150$ km). In such case, the isothermal assumption is fully justified and the above equation simplifies to

$$d^z_\tau = k_1 \frac{R_g P_s}{g_s M}. \quad (10)$$

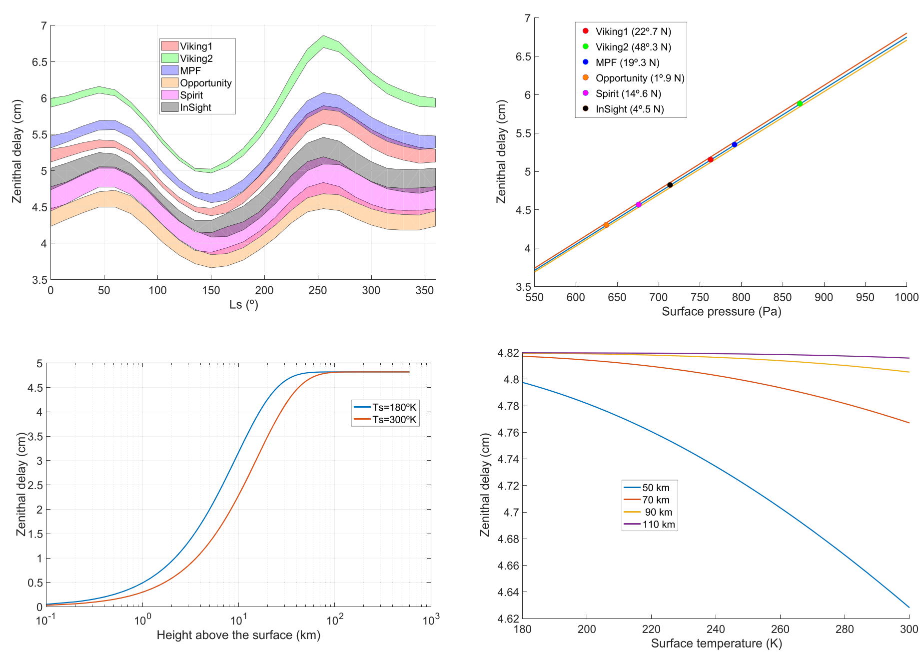

Figure 3. Zenithal delay as a function of Mars longitude (Ls), surface pressure (P_s), receiver altitude (z), and surface temperature (T_s). In bottom panels, d^z_τ has been computed at InSight location, assuming $P_0 = 714$ Pa.

This model of the zenith hydrostatic delay of Mars troposphere is directly proportional to the refractivity constant and the surface pressure at the lander location (see Figure 3) and inversely proportional to the surface gravity acceleration, g_s. g_s depends on the distance to Mars center, d_c. It can easily be computed from the equatorial acceleration, g_0, according to $g_s = g_0 R_e^2 / d_c^2$. For Mars landers, all located at low latitude (60°N-latitude Phoenix lander is not considered in the present study because there is no radio science experiment onboard this lander) (see Folkner et al., 1997, and Table 3), the surface gravity at their location departs from g_0 by up to 0.02 m/s^2 for the northern Viking Lander 2. This induces a negligible variation in d_τ^z of less than 0.5% of its equatorial value. In Figure 3 and in the rest of the paper, d_τ^z is computed from Equation 10 with $g_s = g_0$.

Surface pressure, decreasing with latitude, is the main driver of the Mars troposphere zenithal delay. Closest to the equator, Opportunity has the lowest surface pressure of all landed spacecraft and is therefore less affected by Mars troposphere than the others, with d_τ^z equalling 4.3 cm in average (see Figure 3 top panels). For InSight, d_τ^z is 4.8 cm in average and varies by ±0.7 cm due to variations in P_s (reaching a minimum of about 600 Pa at $Ls = 150°$ and a maximum of about 800 Pa at $Ls = 270°$, see Figure 1). As the highest lander in latitude, Viking Lander 2 experiences the largest troposphere disturbances with d_τ^z reaching 6.8 cm at $Ls = 270°$.

5. Mars Mapping Functions

The propagation delay in the atmosphere of a planet depends on the thickness of the atmosphere crossed by the electromagnetic signal. Thinner when propagating perpendicularly to the ground (when coming from the zenith), this thickness is maximum for grazing raypaths. The delay at the zenith, d_τ^z, therefore corresponds to the minimum delay induced by the troposphere of Mars. The slant delays, systematically larger, are usually computed by multiplying d_τ^z (Equation 10) by a so-called mapping function (m), which models the elevation angle dependence of the propagation delay.

Most of the mapping functions assume an azimuthal symmetry for the atmosphere. In the earlier attempts by Saastamoinen (1972), a simple expression for the mapping function, consistent with a flat atmosphere of the Earth, was examined:

$$m(\epsilon) = \frac{1}{\sin\epsilon}, \tag{11}$$

where ϵ is the raypath elevation angle (between raypath direction and its projection on the local horizon). The subsequent models for Earth troposphere assumed an atmosphere composed of concentric spherical layers. Most of them have been derived from the continued fraction expansion first introduced by Marini (1972):

$$m(\epsilon) = \frac{1}{\sin\epsilon + \frac{a}{\sin\epsilon + \frac{b}{\sin\epsilon + \frac{c}{\cdots}}}}. \tag{12}$$

The coefficients a, b, c, and so forth are estimated from numerical weather models, which makes their determination difficult in the case of Mars. To circumvent this problem, we choose to use the "geometric" mapping function proposed by Foelsche and Kirchengast (2002), which is simple and account for the atmosphere curvature, but does not depend on meteorological data, and/or from weather models:

$$m(\epsilon) = \left(\frac{R_e}{H_{atm}} + 1\right)(\cos(\arcsin(\gamma\cos\epsilon) - \gamma\sin\epsilon). \tag{13}$$

The only free parameter in the above function is an "effective height" of the atmosphere, H_{atm}, which could in practice be estimated along the other target parameters in the least squares procedure used to analyze the Doppler and range data (partial derivatives of these observables with respect to H_{atm} being easy to derive from the equations of the following section). Together with R_e, the Mars equatorial radius, H_{atm} allows to compute the dimensionless ratio γ defined as

$$\gamma = \frac{R_e}{R_e + H_{atm}}. \tag{14}$$

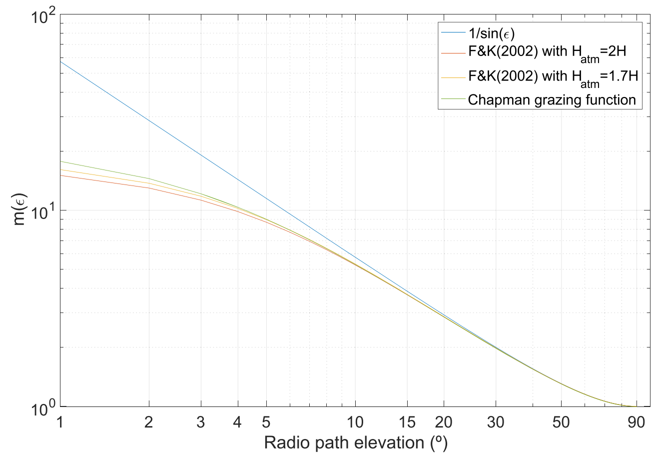

Figure 4. Mapping functions. F&K(2002) stands for Foelsche and Kirchengast (2002).

According to Foelsche and Kirchengast (2002), for the Earth, H_{atm} corresponds to about the first two scale heights (H) above the surface, so we set this parameter to $H_{atm} = 2H = 22.2$ km (see Table 1). We test the validity of this setting for Mars by using the following Chapman function derived by Smith III and Smith (1972) specifically for grazing incidence signal:

$$m(\epsilon) = \sqrt{\frac{\pi(R_e + z)}{2H}} e^{y^2} erfc(y), \quad (15)$$

where *erfc* is the complementary error function, $y = \sqrt{(R_e + z)/(2H)} \sin \epsilon$, and z is the altitude of the observer/target. The mapping function of Foelsche and Kirchengast (2002) best fits the Chapman grazing function at 5° elevation when H_{atm} is set to $\sim 1.7H$, while it best matches the Chapman function at 10° elevation with $H_{atm} = 1.9H$, proving the setting suitable. This can be seen in Figure 4 where the mapping functions described by Equations 11, 13, and 15 are represented as a function the elevation angle of the raypath, as seen from a surface probe. Because the cosecant law (Equation 11) assumes a parallel-plane atmosphere, it overestimates the slant straight-line raypath length, which thus can be seen as the upper limit of Mars troposphere effect in Figure 4 and in the derived quantities presented in the following section and figures. Foelsche and Kirchengast (2002) mapping function shall provide more accurate values at low elevations. For the Earth, Foelsche and Kirchengast (2002) showed that their geometric mapping function generally exhibits a performance comparable to or better than other mapping functions (typically based on equations similar to Equation 12). This statement is valid down to 6° of elevation for the Earth. Below that, the authors observed a marked decrease in the model performance. For Mars, at such an angle, the free parameter H_{atm} makes $m(\epsilon = 6°)$ vary by $\pm 5\%$ of its nominal value when set to $1H = 11.1$ km or $3H = 33.3$ km instead of $2H = 22.2$ km (see the impact of that on the radio observables in the following section). Above that threshold, the dependency of $m(\epsilon)$ to H_{atm} rapidly decreases, already being at about 1% for $\epsilon = 10°$.

6. Mars Troposphere Corrections of Radio Science Data

Spacecraft radio science direct-to-Earth observations mainly consist of range (r) and Doppler (Δf) measurements, which are of three configurations:

- "one-way": when a stable oscillator is present onboard, the spacecraft generates and transmits the radio signal which is recorded by a ground station on Earth.
- "two-way": the radio signal is transmitted by an Earth ground station equipped with high-precision hydrogen maser clock. The spacecraft transponds the signal back to this specific ground station, which generated the uplink frequency used as the reference for the precision Doppler and range measurements.
- "three-way": the ground station receives a signal transponded by the spacecraft, but the uplink is from a different ground station.

In the context of the present study, two- and three-way data are completely identical. Therefore, we do not refer to three-way anymore in the rest of the paper.

6.1. One-Way Measurements

In navigation software, the Doppler observables are modeled using range rates. Range rates ($\dot{r}$) are variations of the transmitter-receiver distance over time, which makes them consistent with measurements of their relative velocity (V_r). For one-way cases, this is expressed as $\dot{r} = V_r = \left(r_e - r_s\right)/t_c$, where t_c is the time used to measure the variation in the range (r). r equals r_s at the start of the time count, and equals r_e at the end of the time count (i.e., after t_c). In order to fit the model to the ground station measurements, the range rate data are converted in frequency measurements (then consistent with Doppler measurements) by multiplying the range rate by the signal carrier frequency (f_c) divided by the speed of light (c):

$$\Delta f_c = \frac{f_c}{c} V_r = \frac{f_c}{c t_c} \left(r_e - r_s\right). \quad (16)$$

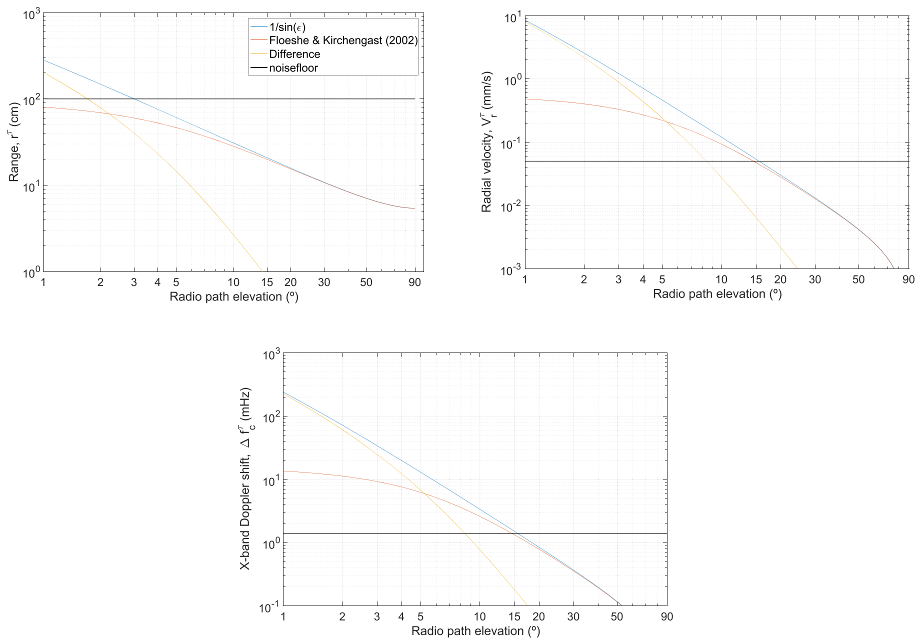

Figure 5. Mars troposphere impact on one-way radio science data as predicted at InSight location by the model (see Equations 17–20), using two mapping functions (see Equations 11–13). The difference in predicted effects by these mapping functions is also plotted. The zenithal delay used for the computation is based on Equation 10 with $P_s = 800$ Pa.

Equation 16 is the mathematical model of a one-way Doppler measurement (Moyer, 2000). According to Equation 16 and the previous sections, the Mars troposphere contributions (pointed out with superscripts τ in the following expressions) to the range, radial velocity, and Doppler measurements are

$$r^\tau = d_\tau^z m(\epsilon), \tag{17}$$

$$V_{r^\tau} = \left(r_e^\tau - r_s^\tau\right) / t_c, \tag{18}$$

$$\Delta f_c^\tau = \frac{f_c}{c} V_{r^\tau}. \tag{19}$$

To clear the radiometric data from the Mars troposphere disturbances, the above quantities have to be removed from the corresponding one-way range, radial velocity, and Doppler observations. All these three observables are functions of the Earth LOS elevation ϵ, which varies with time by an average of ~15° per hour, that is, one fourth of a degree per minute. Since the nominal time count used for lander radio science data analysis is $t_c = 60$ s (Kuchynka et al., 2014; Le Maistre, 2013), one have $|\epsilon_e - \epsilon_s| \simeq 0°.25$, where ϵ_s and ϵ_e are LOS elevation at the start and the end of the time count, respectively. Expressing the one-way Doppler corrections as a function of the model parameters, Equation 19 becomes

$$\Delta f_c^\tau = \frac{f_c d_\tau^z}{c t_c} \left(m(\epsilon_e) - m(\epsilon_s)\right). \tag{20}$$

Figure 5 shows the Mars troposphere impact on one-way radio science data as predicted by the zenithal delay model of section 4, combined with the mapping functions discussed in section 5. The figure exhibits the predicted Mars tropospheric contribution to the range (Equation 17), the radial velocity (Equation 18), and the Doppler shift (Equation 20) observables as a function of the signal elevation. The typical noise level of each quantity is also plotted in Figure 5. For one-way measurements, this corresponds to 1 m for the range, 0.05 mm/s for the radial velocity, and 1.4 mHz for the X-band Doppler shift, assuming V_r and Doppler measurements compressed at $t_c = 60$ s (e.g., Folkner et al., 1997).

As shown in Figure 3, d_τ^z depends on time as it is a function of the surface pressure varying daily and seasonally (see Figure 1). To produce Figure 5, we considered the date when the surface pressure is maximum at

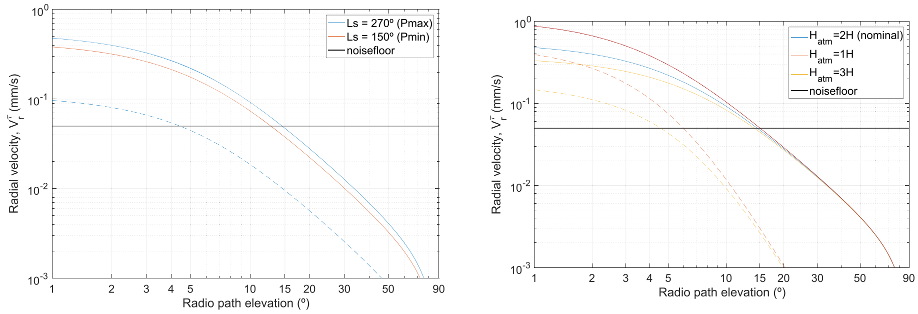

Figure 6. Troposphere-induced radial velocity as a function of the raypath elevation for two end-member surface pressures at InSight (left) and for different effective heights of the atmosphere, H_{atm} (right). Dashed curves are differences between the reference and the case (solid curve) of same color.

InSight location, that is, when $Ls = 270°$ (see Figure 1). Setting P_s to the corresponding 800 Pa, the zenithal delay is calculated to be $d_\tau^z = 5.4$ cm and the slant delay (i.e., r^τ) reaches the meter level at grazing elevations. Because uncertainties in the mapping function, m, propagate in a one-to-one way into r^τ, the tropospheric range corrections predicted by Foelsche and Kirchengast (2002) should be better than 2 cm accuracy at $\epsilon = 6°$ (i.e., 5% level) and should be ∼0.3 cm accurate at $\epsilon = 10°$ (i.e., ∼1% level, see section 5).

Figure 5 also reveals that Mars troposphere range rate (velocity and the inferred Doppler) data compressed at 60 s, shall be corrected if acquired below 15° elevation, since then they rise above the noise floor. Here again, the choice of the mapping function induces uncertainties in the computed velocity and Doppler corrections. Considering the difference, traced in Figure 5, between the simple mapping function ($1/\sin\epsilon$) and the one proposed by Foelsche and Kirchengast (2002), we can conclude that the choice of the mapping function significantly affects the correction to apply to lower-than-8°-elevation radio signals. Above that threshold, corrections predicted by both mapping functions are statistically equivalent. The more sophisticated mapping function of Foelsche and Kirchengast (2002) is nevertheless recommended for real data analysis, especially for low elevation measurements, and is systematically used in the rest of the paper.

Because the troposphere is a non-dispersive medium, the range and radial velocity (or range rate) perturbations are not depending on the radio wave frequency, as clearly understood from Equations 17 and 18. Contrary to this, the magnitude of the Mars troposphere contribution to the Doppler shift is directly proportional to the signal frequency f_c (Equation 20). Δf_c^τ of Figure 5 has been obtained with $f_c = 8.4$ GHz. For a different signal's carrier frequency f, the Mars troposphere contribution to the one-way Doppler would scale directly with f/f_c. Spacecraft radio telecommunication systems commonly uses ultrahigh frequency (UHF), S, X, or Ka frequency bands. For typical frequencies of each of these bands, for instance, $f = 400$ MHz for UHF, $f = 2.1$ GHz for S-band, and $f = 32$ GHz for Ka-band, the X-band signal of Figure 5 would have to be rescaled by 1/21, 1/4, and 3.8, respectively, to reflect the level of contribution of Mars troposphere in each signal. As an example, the 1.4 mHz contribution reached at 15° elevation in X-band would rescale to 0.066 mHz in UHF, 0.35 mHz in S-band and 5.3 mHz in Ka-band still for a 15° elevation raypath.

Figure 6 left panel shows the effect on the radial velocity of the surface pressure variations at InSight location. The minimum pressure leads to 20% lower values for V_{r^τ} than the maximum pressure (used in other figures). This difference is detectable only at elevations smaller than 5°, which would justify using a constant average surface pressure in the computation of d_τ^z for correcting the Doppler data of every Martian landers (see LOS elevation ranges reported in Table 3). This 5° elevation threshold is also the reliability limit of the mapping function as discussed in section 5 and shown on the right panel of Figure 6, where we see that uncertainty of 100% in H_{atm} (which is very conservative) raises above the noise floor at elevation lower than 5–6°.

6.2. Two-Way Measurements

Since most of the radio science instruments onboard landers and rovers do not hold Ultra-Stable-Oscillator (USO), these instruments are not suitable for science operations in one-way mode and the available landers data are thus mostly two-way Doppler data. As said before, the two-way Doppler data involve an uplink (superscripts u), from Earth to Mars, and a downlink (superscripts d), from Mars to Earth.

Table 2
Spacecraft Turnaround Ratio M_{bd} (Moyer, 2000)

Uplink band	Downlink band S	X	Ka
S	240/221	880/221	3,344/221
X	240/749	880/749	3,344/749
Ka	240/3,599	880/3,599	3,344/3,599

The mathematical expression for modeling this kind of measurements is derived from one-way Equation 16 (Moyer, 2000):

$$\Delta f_c^{2w} = \frac{f_c}{ct_c}\left[(r_e^u + r_e^d) - (r_s^u + r_s^d)\right], \tag{21}$$

and the Mars troposphere corrections must be applied on all four radio leg lengths (two r^u and two r^d in Equation 21). If implemented directly in the navigation software used to process the radio-tracking data (like GINS, DPDOP, MONTE, and GEODYN), the tropospheric corrections are range corrections (Equation 17) computed at the correct elevations for each leg. This method is certainly the more precise one but requires implementing the model within the source code of the navigation software, which is not possible for all users. Another way to proceed is by correcting the Doppler data during a preprocessing phase and then analyze the corrected Doppler data with the navigation software. In such a case, the troposphere corrections applies on the frequencies. The one-way correction (Equation 20) must then be extended for two-way observations.

In two-way mode, landed spacecraft transpond the received uplink frequency (f_u) coherently (i.e., without phase shift) but also they generate the downlink frequency (f_d) by multiplying f_u by a constant factor, called *transponder ratio* (M_{bd}). Assuming that no noise is introduced by the transponder on the signal, this means that $f_d = M_{bd} f_u$. M_{bd} only depends on the frequency bands of the uplink and downlink signals. All spacecraft working in a given frequency band must use the same transponder ratio as imposed by the International Telecommunication Union (ITU) and reported in Table 2.

The observed sky frequency f_{obs}^{2w} is recorded at the Earth ground station at a given time t_r^{gs}, which occurs t_L seconds after t_t^{sc}, the time of the signal transmission by the spacecraft (i.e., $t_r^{gs} = t_t^{sc} + t_L$). The exact value of t_t^{sc} is unknown but can be estimated from t_r^{gs} and a precise estimate of the downlink propagation time at light speed, t_L, based on a priori knowledge of the planets ephemeris and rotation, and the antennas location on their surface. The Mars troposphere corrected two-way Doppler measurement can thus be expressed as follows:

$$\Delta f_{cor}^{2w}(t_r^{gs}) = \Delta f_{obs}^{2w}(t_r^{gs}) - \Delta f_u^{\tau}(t_r^{sc}) - \Delta f_d^{\tau}(t_t^{sc}), \tag{22}$$

where t_r^{sc} is the time of reception of the uplink signal by the spacecraft and $\Delta f_u^{\tau}(t_r^{sc})$ and $\Delta f_d^{\tau}(t_t^{sc})$ are one-way Doppler tropospheric corrections computed according to Equation 20, with $f_c = f_u(t_r^{sc})$ and $f_c = f_d(t_t^{sc})$, respectively. Since the transponding time is of a few μs only (Bertone et al., 2018) (i.e., $\ll t_c$), one can consider that $t_r^{sc} = t_t^{sc}$, simply denoted t^{sc} from now on. The sum of the last two terms in Equation 22 corresponds to the total Mars troposphere contribution to the two-way Doppler measurement recorded at t_r^{gs} at the Earth ground station. As a function of the model parameters, this tropospheric correction term reads

$$\Delta f_{\tau}^{2w}(t^{sc}) = \frac{f_u d_{\tau}^z}{ct_c}\left[m(\epsilon_e^u) - m(\epsilon_s^u) + M_{bd}\left(m(\epsilon_e^d) - m(\epsilon_s^d)\right)\right]. \tag{23}$$

f_u and d_{τ}^z are computed at t^{sc}, while elevations are computed at $t^{sc} \pm t_c/2$, depending on the leg: $-t_c/2$ for the ϵ_s, that is, the starting leg elevations, and $+t_c/2$ for the ϵ_e, that is, ending leg elevations. For both uplink and downlink, ϵ^u and ϵ^d must be computed by considering the signal propagation times, t_L^u and t_L^d, respectively. This means that ϵ_e^d and ϵ_s^d, the Earth LOS elevations of the downlink legs, shall be computed considering that the photons departed from the Mars lander's location at the light-time corrected epoch (i.e., $t^{sc} = t_r^{gs} - t_L^d$) and arrived at the observer's location at t_r^{gs}. Similarly, ϵ_e^u and ϵ_s^u, the Earth LOS elevations of the uplink legs, shall be computed such that the photons departed from the Earth transmitting station's location at the light-time corrected epoch (i.e., $t_t^{gs} = t^{sc} - t_L^u = t_r^{gs} - t_L^d - t_L^u$) and arrived at the lander's location at t^{sc}. Note that the $\pm t_c/2$

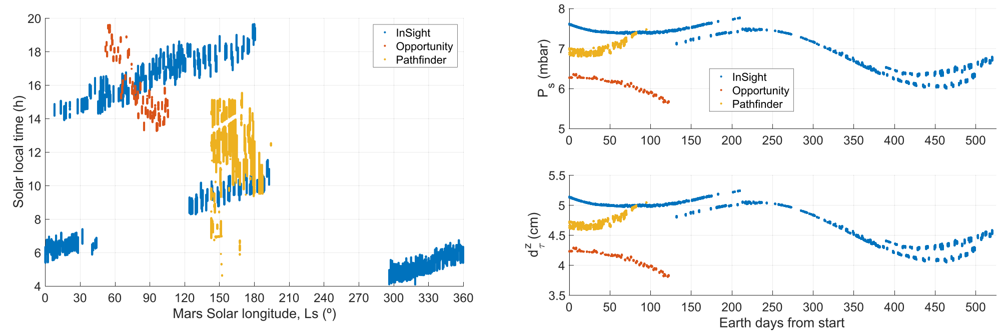

Figure 7. Mars solar longitude versus solar local time (left panel) and surface pressure (top) and zenithal delay (bottom) versus time (right panels) for each X-band Doppler data point of the InSight-RISE, Opportunity, and Pathfinder missions.

terms do not appear in these into-brackets relationships between transmitting and receiving times, because, being in both side of the equal symbol, they cancel out. Such a simplification assumes that t_c, the difference between starting and ending times, is constant. In fact, because the propagation time is not exactly the same at the start and the end of the time count t_c, one should distinguish between $t_c = t^{gs}_{r_e} - t^{gs}_{r_s}$ at Earth receiving station (this is the exact t_c by construction) and $t' = t^{sc}_e - t^{sc}_s$ at Mars or $t''_c = t^{gs}_{t_e} - t^{gs}_{t_s}$ at Earth transmitting station. We nevertheless neglect this distinction which would modify our results in a transparent way since the variations in t_c due to up and down propagation time differences is several orders of magnitude smaller than t_c.

7. Application to the Martian Landers Data

We compute the Mars troposphere contribution to the available two-way Doppler data from Mars landers. Viking Lander 2 Doppler data are not available and Viking Lander 1 Doppler data are discarded because they are in S-band, that is, with a thermal noise about 3 times larger than for the X-band data and with a Mars tropospheric noise 4 times smaller than for the X-band data (see section 6), which make the Mars troposphere calibration of such data totally useless. We therefore focus on the Mars Pathfinder (MPF) 95-day mission, the Mars Exploration Rover (MER) Opportunity 123-day radio science campaign (Between January and May 2012, the DSN conducted Doppler tracking of Opportunity in the framework of the MER Radio Science Tracking Experiment, maintaining the rover was stationary to allow Mars rotation parameters determination; Kuchynka et al., 2014.), and the InSight-RISE mission operating on Mars for more than 500 days now. For each X-band data point of those three missions, we compute the Mars solar longitude (Ls) and solar local time (SLT) at Mars to get the surface pressure from the Global Circulation Model (GCM) (Note that one could use InSight pressure data instead of GCM predictions to calibrate RISE Doppler data. However, model predictions are in very good agreements with InSight observations, with discrepancies between the two having negligible effects on the tropospheric noise.), and we compute the LOS elevation at Mars to infer the troposphere contribution in their Doppler measurements thanks to Equations 10 and 23. Ls and SLT are plotted in Figure 7 left panel, while surface pressure and zenithal delay are shown in Figure 7 right panel. Despite the expected larger zenithal delay for MPF than for the other two (see Figure 3 top panels), Figure 7 right panel shows a larger Mars tropospheric disturbance on RISE data than MPF, which is explained by the fact that MPF operated around Ls = 150°, when the surface pressure, directly proportional to d^z_τ, is minimum (see Figure 1 left panel).

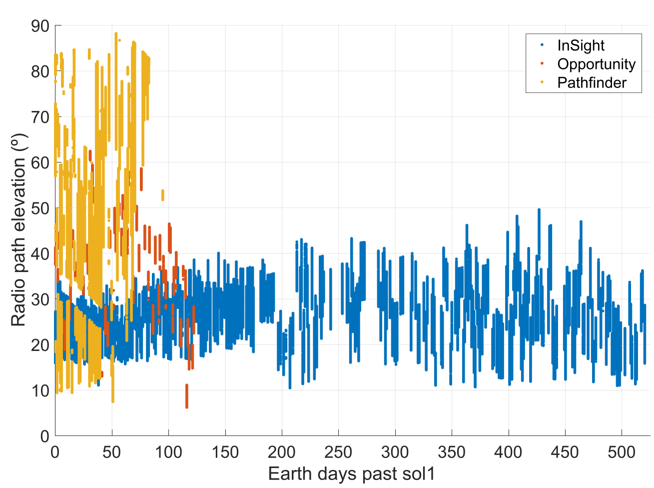

Figure 8. Radio path elevation for each X-band Doppler data point of the InSight-RISE, Opportunity, and Pathfinder missions.

Radio path elevations are plotted as a function of time from the beginning of the mission in Figure 8. Thanks to their steerable high-gain antennas, Pathfinder and Opportunity cover a wide range of LOS elevations, especially MPF, which sometimes was tracked at very high elevation, up to 88° (see Table 3). Both MPF and MER have been tracked at very low elevations, down to 7° and 5°, respectively. Unlike the other two missions,

Table 3
Mars Landed Mission Location and X-Band Doppler Geometry

Rover/lander mission	Time span, mm/yyyy	Latitude (deg)	Longitude (deg)	Distance (d_c) to center (km)	LOS elevation at lander (deg)	LOS elevation ≤15° (%)
Pathfinder	07/1997–10/1997	19°N	33°W	3,389.815	7–88	4.2
Opportunity	01/2012–05/2012	2.2°S	354°E	3,394.056	5–62	2.2
InSight	11/2018, ongoing	4.5°N	136°E	3,393.061	10–50	2.5

InSight has on its main deck two fixed-pointing horn-shape medium-gain antennas (MGAs) (Folkner et al., 2018). One antenna points 5.06° northward from due west, and the other points 16.8° southward from due east, both with the central gain axis at about 30° in elevation above the lander. This allows operating RISE within a limited range of elevations and azimuths (RISE fixed horn antennas aperture is ∼25° from bore sight, Folkner et al., 2018). As a consequence, tracking is sometimes not possible from one of the two MGAs because the Earth does not appear in the antenna field of view every day. RISE is thus sometimes operated from east antenna only, sometimes from west antenna only and sometimes from both antennas, depending on the Martian season, as shown in Figure 7 right panels and Figure 9 right panel, where three branches for RISE can be distinguished.

In Figure 9, one can also notice that the Mars tropospheric Doppler is sometimes positive and sometimes negative. Since Doppler measurements correspond to range rates obtained by integration over a time count (see Equations 16 and 21), if the range at the end of the integration time is less affected by the troposphere than the range at the beginning of the integration time, then the $(r_e^\tau - r_s^\tau)$ difference is negative. This is the case for morning/east tracking sessions with time increasing elevations, since low elevation range measurements have higher Mars troposphere noise than high elevation range measurements. Reciprocally, evening/west tracking sessions result in a positive range difference and Doppler shift because observations are then carried out when LOS elevations are decreasing with time.

For the three missions, the number of data points acquired below the previously identified threshold of 15° of elevation is below 5% (see Table 3 last column). Actually, as shown in Figure 9, the Mars tropospheric Doppler affecting the data raises above the noise floor for less than 1% of RISE data, for barely 2% of MER data and 2.5% of MPF data, which is very low. Nevertheless, for a couple of tracking passes of MER and MPF, the Mars troposphere strongly afflicts the 60 s compressed Doppler data, reaching more than 10 mHz, that is, more than 3 times the nominal noise level (Figure 9).

8. Conclusion

Given the challenging Doppler accuracy required to observe the Mars liquid core contribution in the measurements of RISE or LaRa, it makes sense to endeavor in best calibrating the data. The tropospheric propagation noise is one of several sources of error in radio science measurements. Systematically calibrated for the Earth troposphere disturbances, the ranging and Doppler data have not been corrected so far for Mars troposphere effects, which were assumed negligible with respect to other sources of errors. This assumption has been tested in the present study, where the Mars troposphere effects on the radio-tracking data of

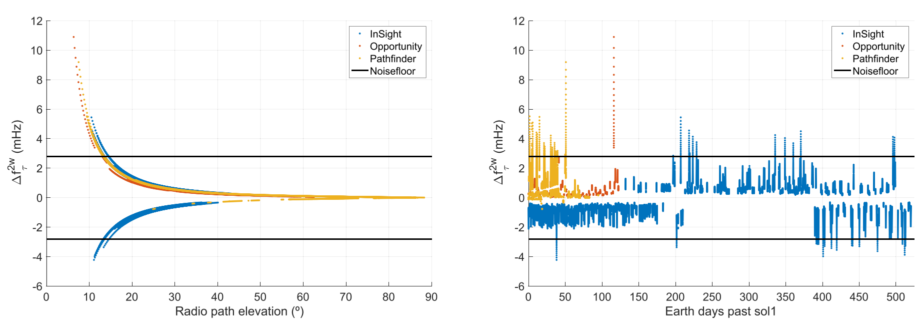

Figure 9. Mars troposphere Doppler contribution for each 60 s compressed X-band Doppler data point of the InSight-RISE, Opportunity, and Pathfinder missions as a function of the LOS elevation (left panel) and time from the beginning of the missions (right panel).

landed probes have been quantified. We proposed a simple model to compute the Mars troposphere propagation zenithal delay, directly proportional to the refractivity constant and the surface pressure at the lander location (deduced from a Mars GCM) and inversely proportional to the surface gravity acceleration. As customary for the Earth, we used a mapping function to project the zenithal delay along the LOS direction to obtain the slant delay. The latter is nothing but the errors in range measurements induced by the troposphere of Mars. Since most of the mapping functions used for the Earth are based on coefficients estimated from numerical weather models, their value for Mars is not straightforward to get. To circumvent this problem, we chose to use the "geometric" mapping function proposed by Foelsche and Kirchengast (2002). This simple model has only one free parameter, which could be estimated along the other target parameters in the least squares procedure used to analyze the Doppler and range data. The function accounts for the Mars atmosphere curvature but does not depend on meteorological data and weather models. Being proportional to range rates, the contribution of Mars troposphere to the Doppler measurements integrated over a typical time of 60 s is obtained from differences in the slant delays at the start and the end of the integration time. Using our model, an elevation threshold of 15° above the lander is identified, below which the 60 s compressed Doppler data should be calibrated for Mars troposphere. When applied to the real X-band Doppler data from Mars surface missions (Pathfinder, Opportunity, and InSight), the model and atmospheric conditions during operations predict significant Mars troposphere contribution for less than 1% of RISE data, for barely 2% of Opportunity data and 2.5% of Pathfinder data. A few tracking passes are strongly afflicted by the troposphere of Mars though, with Doppler errors reaching sometimes more than 10 mHz for Opportunity and Pathfinder, that is, more than 3 times the nominal noise level.

Appendix A: Approximative Two-Way Doppler Models

We provide here two simplified models to correct the two-way Doppler data from Mars troposphere and we assess their respective accuracy with respect to the nominal model proposed and used in this paper (see Equation 23).

A1. Instantaneous Doppler

The relative motion of a transmitter and a receiver causes the received frequency f_r to differ from that of the transmitter, f_t. This difference,

$$\Delta f = f_r - f_t, \tag{A1}$$

characterizes the Doppler effect between any pair of antennas. Accordingly, the uplink (Δf_u) and the downlink Doppler shift (Δf_d) are

$$\Delta f_u = f_{sc} - f_t, \tag{A2}$$

$$\Delta f_d = f_r - f_{sc}, \tag{A3}$$

$$= f_r - (f_t + \Delta f_u). \tag{A4}$$

Given Equation 16 for a one-way link, the above induces

$$\Delta f_{2w} = \Delta f_u + \Delta f_d, \tag{A5}$$

$$= f_t \frac{V_{r_u}}{c} + f_{sc} \frac{V_{r_d}}{c}. \tag{A6}$$

Considering instantaneous Doppler shift, we have $V_{r_u} = V_{r_d} = V_r$, leading to

$$\Delta f_{2w} = f_t \frac{V_r}{c} + (\Delta f_u + f_t) \frac{V_r}{c}, \tag{A7}$$

$$= 2 f_t \frac{V_r}{c} + f_t \left(\frac{V_r}{c} \right)^2. \tag{A8}$$

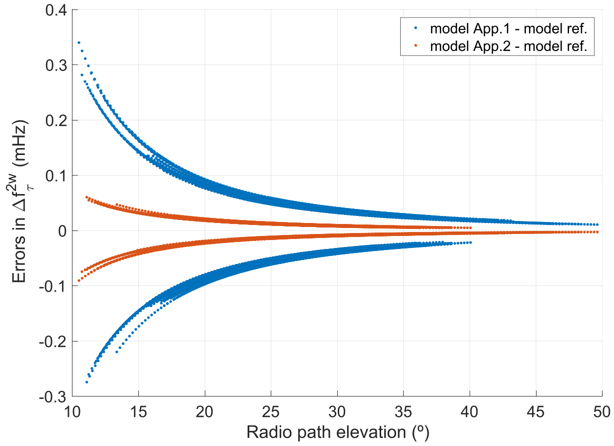

Figure A1. Difference in the Mars troposphere two-way Doppler contributions as computed from Equations A10 and A11 with respect to the reference model of Equation 23.

At first-order approximation in the small quantity $(V_r/c)^2$, Equation A8 simplifies to

$$\Delta f_{2w} = 2 f_t \frac{V_r}{c}, \tag{A9}$$

which is the expression of an instantaneous two-way Doppler shift, simply equal to twice the one-way Doppler shift of Equation 16. Under this assumption of instantaneity of the Doppler, the Mars troposphere contribution in two-way Doppler data reads

$$\Delta f_\tau^{2w} = 2 \frac{f_d d_\tau^z}{c t_c} \left(m(\epsilon_e^d) - m(\epsilon_s^d) \right), \tag{A10}$$

instead of the more correct and complex model of Equation 23. The approximation made with Equation A10 instead of Equation 23 is quantified in Figure A1, where the difference between the Mars troposphere two-way Doppler corrections computed with Equations A10 and 23 is displayed. The ∼15% difference between both models predictions is mostly due to the difference in the uplink and downlink frequencies (i.e., $f_d = M_{bd} f_u$). The correction error induced by such a simple model reaches 0.35 mHz at most, for grazing raypaths. This is one order of magnitude below the typical noise level of X-band measurements.

A2. Uplink and Downlink Elevation Differences

The differences between elevations of the uplink (ϵ^u) and the downlink (ϵ^d) raypaths of RISE is shown in Figure A2 to be always lower than 0.02° in absolute. This leads to a departure from the Δf_τ^{2w} reference value

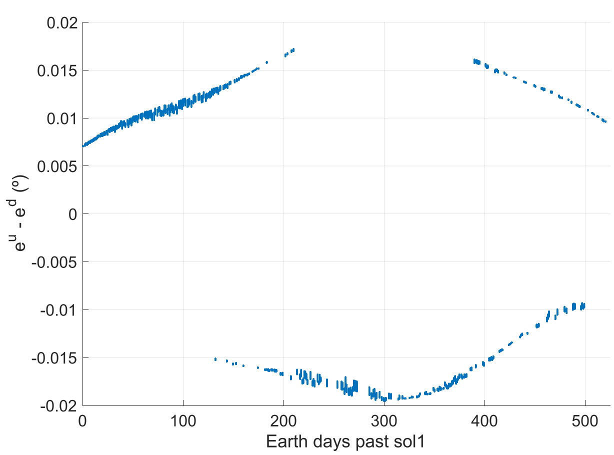

Figure A2. Difference in radio path elevation between uplink and downlink of RISE measurements.

(computed with Equation 23) of about 1% at 10° elevation and 0.5% at 15° elevation. Assuming therefore that $\epsilon^u = \epsilon^d$, Equation 23 becomes

$$\Delta f_\tau^{2w} = \frac{f_u(1+M_{bd})d_\tau^z}{ct_c}\left(m(\epsilon_e^u) - m(\epsilon_s^u)\right). \tag{A11}$$

and the induced difference in Δf_τ^{2w} is of a few tens of μHz, which is negligible in front of the mHz total noise level.

Data Availability Statement

The readers can access to the associated data online (at https://doi.org/10.24414/1bvp-bp73).

Acknowledgments
This work was financially supported by the Belgian PRODEX program managed by the European Space Agency in collaboration with the Belgian Federal Science Policy Office. The author would like to thank C. Nkono and other colleagues from the Royal Observatory of Belgium, with who this work was initiated several years ago.

References

Andrews, D. G. (2010). *An introduction to atmospheric physics* (2nd ed.). New York: Cambridge University Press.

Archinal, B. A., Acton, C. H., A'Hearn, M. F., Conrad, A., Consolmagno, G. J., Duxbury, T., et al. (2018). Report of the IAU working group on cartographic coordinates and rotational elements: 2015. *Celestial Mechanics and Dynamical Astronomy*, *130*(3), 22. https://doi.org/10.1007/s10569-017-9805-5

Asmar, S. W., Armstrong, J. W., Iess, L., & Tortora, P. (2005). Spacecraft Doppler tracking: Noise budget and accuracy achievable in precision radio science observations. *Radio Science*, *40*, RS2001. https://doi.org/10.1029/2004RS003101

Bergeot, N., Witasse, O., Le Maistre, S., Blelly, P. L., Kofman, W., Peter, K., et al. (2019). MoMo: A new empirical model of the Mars ionospheric total electron content based on Mars Express MARSIS data. *Journal of Space Weather and Space Climate*, *9*, A36. https://doi.org/10.1051/swsc/2019035

Bertone, S., Le Poncin-Lafitte, C., Rosenblatt, P., Lainey, V., Marty, J.-C., & Angonin, M.-C. (2018). Impact analysis of the transponder time delay on radio-tracking observables. *Advances in Space Research*, *61*, 89–96. https://doi.org/10.1016/j.asr.2017.09.003

Dehant, V., Le Maistre, S., Baland, R.-M., Karatekin, O., Péters, M.-J., Rivoldini, A., et al. (2020). The radioscience LaRa instrument onboard ExoMars 2020 to investigate the rotation and interior of Mars. *Planetary and Space Science*, *180*, 104776. https://doi.org/10.1016/j.pss.2019.104776

Foelsche, U., & Kirchengast, G. (2002). A simple "geometric" mapping function for the hydrostatic delay at radio frequencies and assessment of its performance. *Geophysical Research Letters*, *29*(10), 1473. https://doi.org/10.1029/2001GL013744

Folkner, W. M., Dehant, V., Le Maistre, S., Yseboodt, M., Rivoldini, A., Van Hoolst, T., et al. (2018). The rotation and interior structure experiment on the InSight mission to Mars. *Space Science Reviews*, *214*(5), 100.

Folkner, W. M., Yoder, C. F., Yuan, D. N., Standish, E. M., & Preston, R. A. (1997). Interior structure and seasonal mass redistribution of Mars from radio tracking of Mars Pathfinder. *Science*, *278*, 1749–1751. https://doi.org/10.1126/science.278.5344.1749

Forget, F., Hourdin, F., Fournier, R., Hourdin, C., Talagrand, O., Collins, M., et al. (1999). Improved general circulation models of the Martian atmosphere from the surface to above 80 km. *Journal of Geophysical Research*, *104*(E10), 24,155–24,176. https://doi.org/10.1029/1999JE001025

Haberle, R., Clancy, R., Forget, F., Smith, M., & Zurek, R. (2017). *The atmosphere and climate of Mars*. Cambridge: Cambridge University Press. https://doi.org/10.1017/9781139060172

Ho, C., Nasser, G., & Kliore, A. J. (2002). Radio wave propagation handbook for communication on and around Mars (*02-5*): Jet Propulsion Laboratory.

Kahan, D., Folkner, W., Buccino, D. R., Dehant, V., Le Maistre, S., Rivoldini, A., et al. (2021). Mars precession rate determined from radiometric tracking of the InSight lander. *Planetary and Space Science*. Under review.

Kleijer, F. (2004). *Troposphere modeling and filtering for precise GPS leveling*. Delft, The Netherlands: NCG, Nederlandse Commissie voor Geodesie, Netherlands Geodetic Commission.

Konopliv, A. S., Asmar, S. W., Folkner, W. M., Karatekin, O., Nunes, D. C., Smrekar, S. E., et al. (2011). Mars high resolution gravity fields from MRO, Mars seasonal gravity, and other dynamical parameters. *Icarus*, *211*, 401–428. https://doi.org/10.1016/j.icarus.2010.10.004

Kuchynka, P., Folkner, W. M., Konopliv, A. S., Park, R. S., Le Maistre, S., & Dehant, V. (2014). New constraints on Mars rotation determined from radiometric tracking of the Opportunity Mars Exploration Rover. *Icarus*, *229*, 340–347. https://doi.org/10.1016/j.icarus.2013.11.015

Le Maistre, S. (2013). The rotation of Mars and Phobos from Earth-based radio-tracking observations of a lander (Ph.D. Thesis), Université Catholique de Louvain.

Le Maistre, S., Péters, M.-J., Marty, J.-C., & Dehant, V. (2020). On the impact of the operational and technical characteristics of the LaRa experiment on the determination of Mars' nutation. *Planetary and Space Science*, *180*, 104766. https://doi.org/10.1016/j.pss.2019.104766

Marini, J. W. (1972). Correction of satellite tracking data for an arbitrary tropospheric profile. *Radio Science*, *7*, 223–231. https://doi.org/10.1029/RS007i002p00223

Mendes, V. B. (1999). Modeling the neutral-atmosphere propagation delay in radio-metric space techniques (Ph.D. Thesis), University of New Brunswick.

Millour, E., Forget, F., Spiga, A., Vals, M., Zakharov, V., Montabone, L., et al. (2018). The Mars climate database (version 5.3). In *From Mars Express to Exomars* (pp. 1–68). Madrid, Spain: ESA-ESAC.

Montmessin, F., Smith, M. D., Langevin, Y., Mellon, M. T., & Fedorova, A. (2017). The water cycle. In R. M. Haberle, R. T. Clancy, F. Forget, M. D. Smith, & R. W. E. Zurek (Eds.), *The atmosphere and climate of Mars*, Cambridge Planetary Science (pp. 338–373). Cambridge: Cambridge University Press. https://doi.org/10.1017/9781139060172.011

Moyer, T. D. (2000). Formulation for observed and computed values of Deep Space Network data types for navigation. [Monograph 2] Deep Space Communications and Navigation Series.

Owen, T., Biemann, K., Rushneck, D. R., Biller, J. E., Howarth, D. W., & Lafleur, A. L. (1977). The composition of the atmosphere at the surface of Mars. *Journal of Geophysical Research*, *82*(28), 4635–4639. https://doi.org/10.1029/JS082i028p04635

Péters, M.-J., Maistre, S. L., Yseboodt, M., Marty, J.-C., Rivoldini, A., Hoolst, T. V., & Dehant, V. (2020). LaRa after RISE: Expected improvement in the Mars rotation and interior models. *Planetary and Space Science*, *180*, 104745. https://doi.org/10.1016/j.pss.2019.104745

Rodin, A. V., Korablev, O. I., & Moroz, V. I. (1997). Vertical distribution of water in the near-equatorial troposphere of Mars: Water vapor and clouds. *Icarus*, *125*, 212–229. https://doi.org/10.1006/icar.1996.5602

Saastamoinen, J. (1972). Atmospheric correction for the troposphere and stratosphere in radio ranging satellites. In *The use of artificial satellites for geodesy* (pp. 247–251). Washington, DC: American Geophysical Union (AGU). https://doi.org/10.1029/GM015p0247

Smith III, F. L., & Smith, C. (1972). Numerical evaluation of Chapman's grazing incidence integral ch (X, Ï). *Journal of Geophysical Research*, *77*(19), 3592–3597. https://doi.org/10.1029/JA077i019p03592

Smith, E. K., & Weintraub, S. (1953). The constants in the equation for atmospheric refractive index at radio frequencies. *Proceedings of the IRE*, *41*(8), 1035–1037. https://doi.org/10.1109/JRPROC.1953.274297

Withers, P. (2010). Prediction of uncertainties in atmospheric properties measured by radio occultation experiments. *Advances in Space Research*, *46*(1), 58–73. https://doi.org/10.1016/j.asr.2010.03.004